Eur. Phys. J. A **26**, 327–332 (2005)
DOI 10.1140/epja/i2005-10179-x

THE EUROPEAN PHYSICAL JOURNAL A

Bimodality and charge splitting in fission of actinides

A.V. Andreev[1,2], G.G. Adamian[1,3,a], N.V. Antonenko[1,2], and S.P. Ivanova[1]

[1] Joint Institute for Nuclear Research, 141980 Dubna, Russia
[2] Institut für Theoretische Physik der Justus-Liebig-Universität, D-35392 Giessen, Germany
[3] Institute of Nuclear Physics, Tashkent 702132, Uzbekistan

Received: 16 August 2005 / Revised version: 14 November 2005 /
Published online: 16 December 2005 –
Communicated by D. Guerreau

Abstract. Within the scission point model the bimodality in fission of actinides is demonstrated to be related to different neighboring charge and mass splittings. This phenomenon is peculiar not only for the fission of heavy nuclei like ^{256,258}Fm and ^{256,258,262}No but also for fission of lighter actinides like ^{236}U, ^{240}Pu and ^{252}Cf. The experiments are suggested to prove our interpretation of bimodality.

PACS. 24.75.+i General properties of fission – 21.60.Gx Cluster models

1 Introduction

The experiments [1–3] have revealed the interesting spontaneous-fission properties of fermium ^{258,259}Fm and transfermium ^{259,260}Md, ^{258,262}No nuclides in which the total-kinetic-energy (TKE) distributions of the fragments appeared to be composed of two Gaussians with the maxima near 200 and 230 MeV. As was determined, the highest energy TKE is associated with sharply symmetrical mass distribution, while the lower-energy fragments produce broadly symmetrical and in some cases asymmetrical mass distribution. Since it appears that each distribution arises from a separate mode of fission, this phenomenon is called bimodal fission.

The possible explanation of the bimodal fission comes from the analysis of the potential energy surface of the fissioning system as a function of deformation parameters [4–8]. The microscopic calculations on the basis of the constrained Hartree-Fock-Bogoliubov theory and Gogny's force [7,8] show a few well-defined paths corresponding to different fission modes. In spontaneous fission after penetration through the first fission barrier the fissioning system can move along two trajectories in the deformation space. One leads to the compact configuration and high-TKE mode, the other to the highly deformed or elongated configuration and low-TKE mode. However, the probabilities to catch each trajectory as well as the transitions between the trajectories were treated rather qualitatively. As a rule, the charge asymmetry of scission configurations was not an independent collective coordinate but rigidly related to the mass asymmetry. In this case one cannot distinguish different charge splittings at given mass division.

In the experiments the number of fission modes is defined from the analysis of TKE mass distributions, *i.e.* from the analysis of possibilities of realization of various scission configurations. As follows from the microscopic treatment of fission dynamics in ref. [9], the fission characteristics considered below are well determined by the scission configurations. In present paper we describe the bimodal fission with the scission point model [10,11]. This model shows that the shell effects in the forming fragments play an important role in determining fission observables. The validity of the scission point model was demonstrated in ref. [11] in the good description of the TKE and relative yields of fission fragments and in the evident explanation of the recently observed fine structure of the TKE mass distribution of fission fragments [12]. It is necessary to stress that in comparison to ref. [10] our model allows us to define strictly the internuclear distance R and excitation energy E^* in the scission configuration. With this model, where the charge asymmetry is easily introduced as independent variable, one can check the idea that two different fission modes are produced by the fragmentations with different charge (mass) asymmetry. If one of the fragments is ^{132}Sn, on the potential energy surface as a function of deformations of the fragments one can expect a deep minimum corresponding to compact configuration with short distance between charge-centers of fragments and high TKE of the fragments after scission due to the strong Coulomb repulsion. If we slightly change the charge asymmetry, the minimum on the potential energy surface can be sharply shifted to larger values of deformations of the fragments. This leads to the more elongated scission configuration and low TKE.

[a] e-mail: adamian@thsun1.jinr.ru

2 Model

The fissioning nucleus with mass A and charge Z can be described at the scission point as dinuclear systems (DNS) with the two fission fragments in contact. Typical characteristics of the DNS are the excitation energy E^*, the charge ($Z_L, Z_H = Z - Z_L$) and mass ($A_L, A_H = A - A_L$) numbers, and the deformation parameters (β_L, β_H) of light (L) and heavy (H) nuclei, respectively, determine the mass, charge and kinetic-energy distributions of the fission fragments. We treat the fragment pairs as nearly touching, coaxial prolate ellipsoids [10]. The deformation parameters β_i are defined as the ratios of the major (c_i) and minor (a_i) semiaxes of the ellipsoids, $i = L$ or H. The volume conservation is taken into consideration. The used shape parameterization is appropriate for studying shapes with well-developed necks that correspond to the scission configurations.

As follows from the experimental study [13], at moderately high TKE the nuclear charge-division at a constant mass ratio A_L/A_H is determined not only by the asymptotic Q-values, but by the potential energy at the scission point [10,11]. So, the crucial point of our treatment is the calculation of the potential energy U which is the sum of the liquid-drop ($U^i_{\rm LD}$) and microscopic shell correction ($\delta U^i_{\rm sh}$) energies for each DNS nucleus, and of the Coulomb ($V_{\rm C}$) and nuclear ($V_{\rm N}$) potential terms describing the interaction between the DNS nuclei:

$$\begin{aligned} U(\{A_i, Z_i, \beta_i\}, R, E^*) = \\ U^L_{\rm LD}(A_L, Z_L, \beta_L) + U^H_{\rm LD}(A_H, Z_H, \beta_H) \\ +\delta U^L_{\rm sh}(A_L, Z_L, \beta_L, E^*) + \delta U^H_{\rm sh}(A_H, Z_H, \beta_H, E^*) \\ +V_{\rm C}(\{A_i, Z_i, \beta_i\}, R) + V_{\rm N}(\{A_i, Z_i, \beta_i\}, R). \end{aligned} \quad (1)$$

The Coulomb potential $V_{\rm C}$ is calculated with the method given in ref. [14]. The calculation of $V_{\rm N}$ is performed in the double-folding procedure with Skyrme-type density-dependent nucleon-nucleon forces [15] using the parameter of nuclear radius $r_0 = 1.15$ fm and the diffuseness parameter $a = 0.55$ fm. The liquid-drop parts are calculated like in ref. [11] with the parameters listed in ref. [16]. The two-center shell model [17] is used to calculate the microscopic shell corrections $\delta U^i_{\rm sh}$. The details of potential energy calculations are presented in ref. [11].

The decaying DNS starting at the touching distance $R_m \approx c_L + c_H + 0.5$ fm has to overcome a small potential barrier $\Delta V = U(R_b) - U(R_m)$ at $R_b \approx c_L + c_H + 1.5$ fm [15, 18] which results from the sum of the attractive nuclear and repulsive Coulomb potentials. This barrier keeps the DNS nuclei in contact and allows the DNS nuclei to take statistical distributions in the space (β_L, β_H). At 1.5 fm between the nuclear surfaces only the variation of the deformations of nuclei is important and taken into account. The additional shape variation at smaller distances can decrease the potential energy but remains this barrier. The barrier resulting from our calculations is consistent with the existence of third minima found experimentally [19] in some heavy nuclei and with the shell model and macroscopic-microscopic calculations [20]. It was earlier mentioned in ref. [21] that the qualitative reason for such a third well is the complete formation of the fragments at the scission point. Our calculations of the potential energy of scission point configurations seem to be more appropriate than the liquid-drop calculations where the nuclear part of the interaction is simulated by a relatively large neck for which various phenomenological criteria of sudden rupture are assumed. In these liquid-drop calculations the statistical equilibrium in deformations is reached due to quite a large time of descent from the saddle point to scission because of the large viscosity.

The values of ΔV in the considered DNS are less than 2 MeV for ^{236}U and ^{240}Pu, and less than 0.5 MeV for Fm and No. It is interesting to compare our results with the potential energy calculations within the self-consistent microscopic model in refs. [7,8]. If we take spherical fission fragments of ^{258}Fm and calculate the quadrupole moment Q_2 of the DNS at $R = R_m$ and R_b, we obtain $Q_2 = 95$ and 110 m_0 b, respectively, using the definition of Q_2 in ref. [7] (m_0 is the nucleon mass). For $95 \le Q_2 \le 110$, in fig. 6 of ref. [7] the dependence of the potential on Q_2 is rather weak. In our case the potential is also flat in this region of Q_2 because of the competition between the repulsive Coulomb and attractive nuclear interactions. We get the shallow potential minimum of the depth of about 0.5 MeV while there is no pocket in fig. 6 of ref. [7]. This disagreement is probably related to the stronger nuclear attraction between the fragments in our case.

The value of ΔV depends on the deformations of the fragments. With the used shape parameterization of the DNS nuclei the value of ΔV decreases with increasing β_L and β_H. For the nearly symmetric mass splittings considered, we do not treat β_L and β_H larger than 1.95 because these configurations are without a potential barrier ($\Delta V = 0$) which prevents the immediate decay of the DNS. The quadrupole moment of an ellipsoid with $\beta = 1.95$ is equal to the quadrupole moment of a nucleus with a quadrupole deformation parameter of about 0.6 if one uses the expansion of the nuclear surface in spherical functions.

At fixed mass and charge splittings $\{A_i, Z_i\}$ the total kinetic energy of the fission fragments is defined as

$$\begin{aligned} {\rm TKE}(\{A_i, Z_i, \beta_i\}) = V_{\rm C}(\{A_i, Z_i, \beta_i\}, R_b) \\ +V_{\rm N}(\{A_i, Z_i, \beta_i\}, R_b). \end{aligned} \quad (2)$$

The excitation energy of the scission configuration is related to the Q-value as follows:

$$\begin{aligned} E^*(\{A_i, Z_i, \beta_i\}, R_b) = Q - {\rm TKE}(\{A_i, Z_i, \beta_i\}) \\ +S - E_{\rm def}(\{A_i, Z_i, \beta_i\}, E^*), \end{aligned} \quad (3)$$

where $E_{\rm def}$ is the deformation energy coming from the deviation of β_i from the values corresponding to the ground states of the DNS nuclei and $S = S_n \approx 8$ MeV the excitation energy coming from the thermal neutron in the neutron-induced fission. In spontaneous fission $S = 0$.

In order to calculate the relative primary (before evaporation of neutrons) yields Y of fission fragments, we use the following expression of the statistical treatment [10]:

$$Y(\{A_i, Z_i, \beta_i\}) = Y_0 \exp(-U(\{A_i, Z_i, \beta_i\}, R_m, E^*)/T), \quad (4)$$

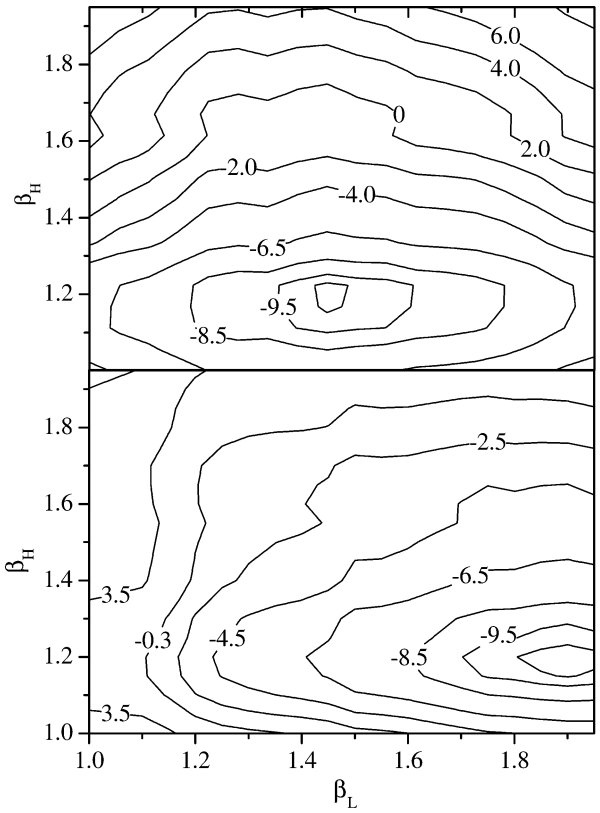

Fig. 1. Potential energies of scission configurations ($R = R_b(\beta_L, \beta_H)$) as functions of β_L and β_H for the spontaneous fission of ^{258}Fm leading to ^{126}Sn + ^{132}Sn (upper part) and ^{124}Cd + ^{134}Te (lower part). The potential energy in MeV is calculated with respect to the ground-state energy of ^{258}Fm.

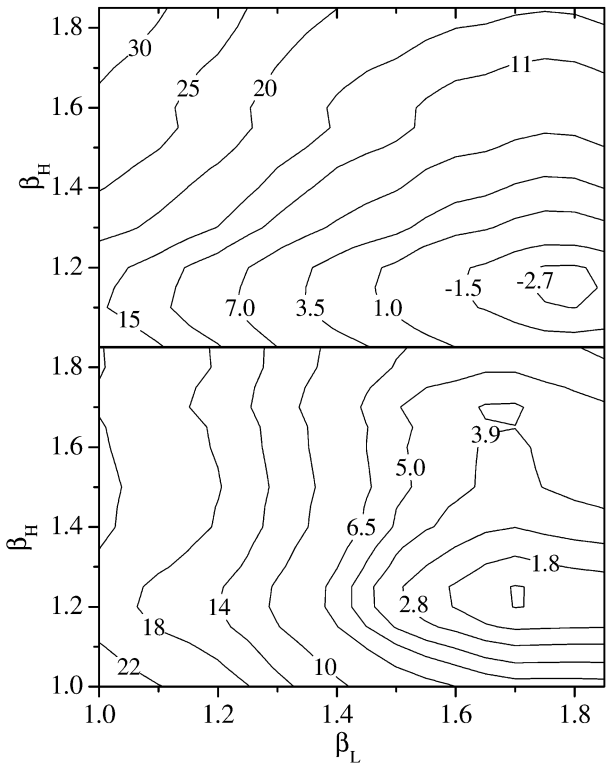

Fig. 2. The same as in fig. 1, but for neutron-induced fission of ^{235}U leading to ^{104}Mo + ^{132}Sn (upper part) and ^{104}Zr + ^{132}Te (lower part). The potential energy in MeV is calculated with respect to the ground-state energy of ^{236}U.

where Y_0 is the normalization factor. In eq. (4), $T = (E^*/a)^{1/2}$ ($a = A/12$ MeV^{-1}) is the temperature at the scission configuration which has the minimal potential energy among the configurations considered [11]. The secondary (after evaporation of neutrons) yields of fission fragments can be calculated using the excitation energy E^*_L (E^*_H) of the fission fragments. E^*_L (E^*_H) consists of the excitation energy of the fragment at scission and the deformation energy which is transferred into the internal excitation after scission. The excitation energy E^* of the scission configuration is assumed to be distributed between the fragments proportional to their masses.

3 Results of calculations

For each mass and charge splittings, we analyze the potential energy surface of the DNS as a function of the deformations of two fragments. Due to the shell effects, the potential energy surface can have one or several minima at some β_L and β_H. Based on the statistical approach one concludes that the DNS decays with larger probabilities from the configurations with these β_L and β_H [11]. If the neutron and/or charge numbers of the fragment are close to the magic numbers, the potential energy surface has quite a deep minimum corresponding to a small deformation of this fragment due to the strong shell effects. In this case the scission configuration is compact which leads to high TKE of the fission fragments. If two fragments are not the magic nuclei, the deepest minima correspond to large values of β_L and β_H and we deal with the elongated scission configuration and, thus, with low TKE values.

This is illustrated in figs. 1, 2 and table 1, for example, for the fragmentations ^{258}Fm (sf) $\rightarrow$ ^{126}Sn + ^{132}Sn ($Z_L = Z_H = 50$) and ^{124}Cd + ^{134}Te ($Z_L = 48$, $Z_H = 52$), and ^{235}U($n_{\rm th}$,f) $\rightarrow$^{104}Mo + ^{132}Sn ($Z_L = 42$, $Z_H = 50$) and ^{104}Zr + ^{132}Te ($Z_L = 40$, $Z_H = 52$). In the scission configurations the deformations of double magic ^{132}Sn and magic ^{134}Te do not exceed 1.15 and 1.2, respectively. In the DNS the non-magic nuclei ^{104}Zr, ^{104}Mo, ^{124}Cd and ^{132}Te can be strongly deformed ($\beta_i = 1.7$–1.9) because of the weaker shell effects. While in the case of ^{126}Sn + ^{132}Sn the potential minimum corresponds to the compact configuration with $\beta_L = 1.4$ and $\beta_H = 1.15$, in the case of ^{124}Cd + ^{134}Te it corresponds to the elongated configuration with $\beta_L = 1.9$ and $\beta_H = 1.2$. The potential energies in these minima are almost the same, which means the comparable yields of fragments with high (230 MeV) and low (209 MeV) TKE (table 1). The configuration ^{126}Cd + ^{132}Te, which contributes also to the low-TKE mode with TKE = 207 MeV ($Y = 0.14$) and 194 MeV ($Y = 0.01$), is presented in table 1 as well. The experimental high- and low-TKE modes are characterized by TKE = 230 MeV,

Table 1. Calculated characteristics of some scission configurations in the indicated fissioning nuclei.

Fissioning nucleus	Scission configuration	β_L	β_H	TKE (MeV)	Y	E^*_L (MeV)	E^*_H (MeV)
^{262}No (sf)	^{130}Te + ^{132}Sn	1.7	1.15	225	0.78	24.6	15.6
	^{128}Sn + ^{134}Te	1.3	1.2	238	0.004	17.7	10.2
	^{128}Cd + ^{134}Xe	1.9	1.35	213	0.014	29.6	13
		1.9	1.7	200	0.082	30.7	24.8
	^{126}Cd + ^{136}Xe	1.9	1.25	216	0.12	30	13
^{258}No (sf)	^{128}Sn + ^{130}Te	1.3	1.7	222	0.08	13.5	23
	^{126}Cd + ^{132}Xe	1.85	1.7	202	0.075	29	22
	^{124}Cd + ^{134}Xe	1.9	1.35	212	0.075	29.3	15
		1.9	1.7	200	0.41	31.3	25
	^{122}Cd + ^{136}Xe	1.9	1.25	215	0.36	30.5	13
^{256}No (sf)	^{126}Sn + ^{130}Te	1.4	1.7	217	0.023	19.2	25
	^{124}Cd + ^{132}Xe	1.9	1.7	200	0.034	30.8	23
	^{122}Cd + ^{134}Xe	1.9	1.35	212	0.09	29.9	14.6
		1.9	1.7	200	0.80	31.7	24.8
	^{120}Cd + ^{136}Xe	1.9	1.25	215	0.053	28.2	15
^{258}Fm (sf)	^{126}Sn + ^{132}Sn	1.4	1.15	230	0.4	13.7	9.3
	^{124}Cd + ^{134}Te	1.9	1.2	209	0.45	30.3	10.2
	^{126}Cd + ^{132}Te	1.9	1.25	207	0.14	30.4	10.5
		1.9	1.7	194	0.01	27.9	26
^{256}Fm (sf)	^{124}Sn + ^{132}Sn	1.45	1.15	225	0.18	14.8	10.5
	^{124}Cd + ^{132}Te	1.9	1.25	207	0.53	29.8	10.6
		1.9	1.7	194	0.04	27.4	26
	^{126}Cd + ^{130}Te	1.85	1.7	194	0.26	27.7	23.4
^{252}Cf (sf)	^{120}Cd + ^{132}Sn	1.9	1.15	202	0.59	22.6	12
	^{118}Pd + ^{134}Te	1.85	1.2	198	0.28	20.3	11.6
	^{120}Pd + ^{132}Te	1.9	1.25	199	0.12	21	12
		1.85	1.7	187	0.01	16.2	28.8
^{239}Pu($n_{\rm th}$,f)	^{108}Ru + ^{132}Sn	1.85	1.15	189	0.73	13.8	15.6
	^{106}Mo + ^{134}Te	1.85	1.2	187	0.16	14.5	15.2
	^{108}Mo + ^{132}Te	1.7	1.25	189	0.1	11.3	14.2
		1.7	1.7	176	0.01	10.2	28.3
^{235}U($n_{\rm th}$,f)	^{104}Mo + ^{132}Sn	1.8	1.15	184	0.75	11.6	12.3
	^{102}Zr + ^{134}Te	1.75	1.2	181	0.22	9.6	14
	^{104}Zr + ^{132}Te	1.7	1.25	181	0.029	8.2	12.8
		1.7	1.7	168	0.001	8	26

$Y = 0.5$ and TKE = 205 MeV, $Y = 0.5$, respectively [1]. So, in contrast to the lighter actinides, a dramatic shift towards symmetric mass distributions accompanied with a high kinetic-energy release is observed for spontaneous fission of ^{258}Fm [1,2]. In the fission of ^{236}U, the relatively compact (TKE = 184 MeV) configuration ^{104}Mo + ^{132}Sn has smaller potential energy in the minimum at $\beta_L = 1.8$ and $\beta_H = 1.15$ than the potential energies of the system ^{104}Zr + ^{132}Te in the relatively compact (TKE = 181 MeV) and elongated (TKE = 168 MeV) minima at $\beta_L = 1.7$, $\beta_H = 1.25$ and $\beta_L = \beta_H = 1.7$, respectively. The calculated ratios of the yields of ^{104}Mo and ^{104}Zr listed in table 1 are in agreement with the experimental one within the error bars. The experiment gives $Y(^{104}\text{Mo})/Y(^{104}\text{Zr}) = (59.4 \pm 3.1)/(5.9 \pm 1.7)$ at TKE = 184 MeV and $(72.3 \pm 3.6)/(3.5 \pm 1.4)$ at TKE = 176 MeV [22].

Thus, the small variations of Z_L (Z_H) and A_L (A_H) lead to quite a large change of the TKE of fission fragments. We suggest that different splittings are separately responsible for the high and low regions of the TKE distribution of fission fragments. So, the bimodality of fission of

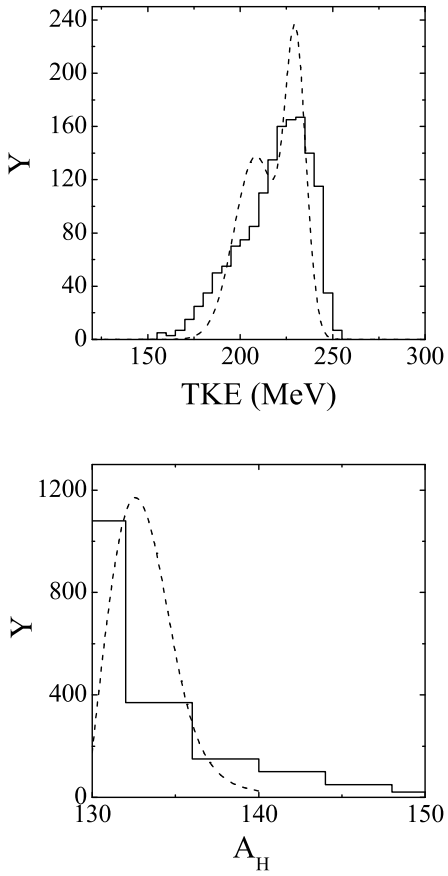

Fig. 3. The calculated (dashed curves) kinetic-energy distribution (upper part) and mass distribution (lower part) of fission fragments of ^{258}Fm are compared with the experimental data (histogram) [1].

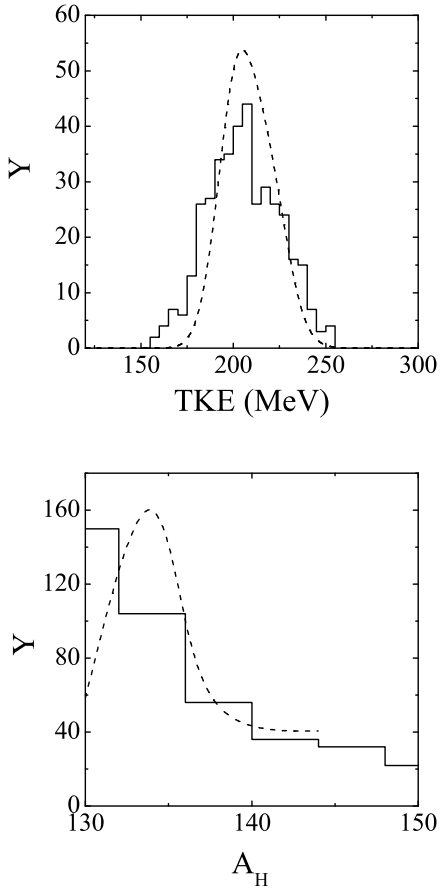

Fig. 4. The same as in fig. 3, but for the fission fragments of ^{258}No.

heavy actinides can be related to different neighboring values Z_L (Z_H). The corresponding mass numbers A_L (A_H) are close or equal to each other. The examples of this in the fission of ^{256}Fm and ^{256,258,262}No are given in table 1. For instance, in the fission of ^{262}No (^{256}Fm) the high- and low-TKE modes correspond to the configurations $^{262}\text{No} \to {}^{130,134}\text{Te} + {}^{132,128}\text{Sn}$ ($^{256}\text{Fm} \to {}^{124}\text{Sn} + {}^{132}\text{Sn}$) and $^{262}\text{No} \to {}^{128,126}\text{Cd} + {}^{134,136}\text{Xe}$ ($^{256}\text{Fm} \to {}^{124,126}\text{Cd} + {}^{132,130}\text{Te}$), respectively.

In table 1 one can see the dramatic difference between ^{262}No (^{258}Fm) and ^{256,258}No (^{256}Fm). Among the considered nuclei having almost symmetric mass distribution of the fission fragments, the calculated relative yield of ^{132}Sn as a primary fission fragment is large only for ^{258}Fm and ^{262}No (table 1). For ^{256}Fm and ^{256,258}No, the maxima of the fission yields are shifted towards ^{130,132}Te and ^{134}Xe, respectively, which mainly contribute to the low-TKE mode. The global trend is that the weight of the scission configuration with ^{132}Sn producing the high-TKE fission mode grows with increasing N/Z ratio in isotopes of Fm and No. In the fission of ^{262}No, the experimental [3] weight of the high-TKE ($\approx$ 220–235 MeV) mode is comparable and even larger than the weight of the low-TKE mode ($\approx$ 200 MeV) [3]. In addition, it seems that different modes of fission compete with each other. In contrast to ^{262}No and ^{258}Fm, for nuclei ^{256,258}No and ^{256}Fm both the mass and kinetic-energy distributions are more consistent with systematics observed for lighter actinides. For ^{258}No, the experiment [1] gives TKE = 232 MeV, $Y = 0.05$ and TKE = 204 MeV, $Y = 0.95$ for high- and low-TKE modes, respectively. In the case of ^{256}Fm the calculated TKE = 194–207 MeV are in agreement with the experimental data [2].

In comparison to ref. [11], we consider here the fission splittings near ^{132}Sn which do not correspond to the scission configurations contributing to the maximum of the mass distributions of the fission fragments of ^{236}U, ^{240}Pu and ^{252}Cf. As a result, the relative yields listed in table 1 are not the same as in ref. [11] some insignificant misprints of which are corrected in the present paper. Contrary to Fm and No, in ^{236}U, ^{240}Pu and ^{252}Cf the complementary fragments to ^{132}Sn or ^{134}Te are far from the magic nucleus and can be considerably deformed. Therefore, the TKE in the high-TKE mode differs not much from the TKE in the low-TKE mode which has relatively large yield (table 1). The calculated ratio of the yields of ^{108}Ru and ^{108}Mo in the fission of ^{240}Pu is in agreement with the experimental ratios: $Y(^{108}\text{Ru})/Y(^{108}\text{Mo}) = (52.2\pm5.1)/(16.8\pm1.8)$ at TKE = 192 MeV and $(63.9\pm4.5)/(9.1\pm0.7)$ at TKE = 185 MeV [23].

In the scission configurations of ^{236}U, ^{240}Pu and ^{252}Cf with ^{132}Te as heavy fragment there are two pronounced potential minima at ($\beta_L = 1.7$, $\beta_H = 1.25$) and ($\beta_L = 1.7$, $\beta_H = 1.7$) leading to the high- and low-TKE modes, respectively. These are examples of two modes of deformation at the same charge and mass asymmetries. The decays from the minima with $\beta_H = 1.25$ lead to almost the same TKE like in the scission of the relatively compact configurations with ^{132}Sn or ^{134}Te. The yields of low-TKE components from the minima with $\beta_H = 1.7$ are very small, which can create some difficulties in their identifications. Analogously there are two modes of deformation (at the same charge and mass asymmetries) in the following fragmentations of heavy actinides (table 1): ^{262,258,256}No $\rightarrow$ ^{128,124,122}Cd + ^{134}Xe and ^{258,256}Fm $\rightarrow$ ^{126,124}Cd + ^{132}Te. In the contrast to lighter actinides, these modes are regarded only to the low-TKE regime.

Considering nearly symmetric scission configurations and using eq. (4), the mass distributions of fission fragments of ^{258}Fm and ^{258}No are calculated and compared with the experiment in figs. 3 and 4. Taking into account the experimental uncertainty in the determination of the mass of the fission fragment, one conclude about the satisfactory agreement between the calculated and experimental results. Approximating the kinetic-energy distribution by the Gaussian [11] for each scission configuration of ^{258}Fm and ^{258}No listed in table 1, we calculate the kinetic-energy distributions of the fission fragments (figs. 3 and 4) which are in good agreement with the experiment.

4 Summary

In conclusion, the bimodality or multimodality of fission can be related to the variations of the charge and mass splittings in the small interval of charge and mass numbers. In order to obtain high- and low-TKE regimes in the fissioning nucleus, one should not always require two fission paths, short and long, at the fixed charge and mass asymmetries. The suggested explanation of bimodal fission is rather simple and allows us to describe well the available experimental data. This explanation can be experimentally checked by measuring the masses and charges of the fission products along with their kinetic energies. The identification of Z_L (Z_H) and mass numbers after the de-excitation of the fragments with γ-spectroscopy is very promising. The neutron evaporation from the fragments can be estimated with the average values of excitation energies of the fragments listed in table 1. The suggested observation of bimodality requires the precise determination of the masses of primary fragments. Additionally, one can expect different angular momenta of the fission fragments for different modes to be measured.

We thank Professor R.V. Jolos, Professor Yu.V. Pyatkov, Professor W. Scheid, and Professor V.V. Volkov for fruitful discussions and suggestions. A.V.A. thanks the European Physical Society for the support. This work was supported in part by DFG (Bonn), RFBR (Moscow), Volkswagen-Stiftung (Hannover), and Polish-JINR (Dubna) and IN2P3-JINR (Dubna) Cooperation Programmes.

References

1. E.K. Hulet *et al.*, Phys. Rev. C **40**, 770 (1989); Phys. Rev. Lett. **56**, 313 (1986).
2. H.C. Britt, D.C. Hoffman, J. van der Plicht, J.B. Wilhelmy, E. Cheifetz, R.J. Dupzyk, R.W. Lougheed, Phys. Rev. C **30**, 559 (1984).
3. E.K. Hulet, in *Proceedings of the 3rd International Conference on Dynamical Aspects of Nuclear Fission, Casta-Papiernucka, Slovak Republic, 1996*, edited by J. Kliman, B.I. Pustylnik (JINR Publishing Department, Dubna, 1996).
4. P. Möller, J.R. Nix, W.J. Swiatecki, Nucl. Phys. A **469**, 1 (1987); **492**, 349 (1989).
5. V.V. Pashkevich, Nucl. Phys. A **477**, 1 (1988).
6. S. Cwiok, P. Rozmej, A. Sobiczewski, Z. Patyk, Nucl. Phys. A **491**, 281 (1989).
7. M. Warda, J.L. Edigo, L.M. Robledo, K. Pomorski, Phys. Rev. C **66**, 014310 (2002).
8. M. Warda, K. Pomorski, J.L. Edigo, L.M. Robledo, Int. J. Mod. Phys. E **13**, 169 (2004).
9. H. Goutte, J.F. Berger, P. Casoli, D. Gogny, Phys. Rev. C **71**, 024316 (2005).
10. B.D. Wilkins, E.P. Steinberg, R.R. Chasman, Phys. Rev. C **14**, 1832 (1976).
11. A.V. Andreev, G.G. Adamian, N.V. Antonenko, S.P. Ivanova, W. Scheid, Eur. Phys. J. A **22**, 51 (2004).
12. Yu.V. Pyatkov, V.G. Tishchenko, V.V. Pashkevich, V.A. Maslov, D.V. Kamanin, I.V. Kljuev, W.H. Trzaska, Nucl. Instrum. Methods A **488**, 381 (2002).
13. U. Quade *et al.*, Nucl. Phys. A **487**, 1 (1988).
14. R.W. Hasse, W.D. Myers, *Geometrical Relationships of Macroscopic Nuclear Physics* (Springer-Verlag, Berlin, 1988).
15. G.G. Adamian *et al.*, Int. J. Mod. Phys. E **5**, 191 (1996).
16. W.P. Myers, W. Swiatecki, Ark. Fys. **36**, 343 (1967).
17. J. Maruhn, W. Greiner, Z. Phys. **251**, 431 (1972); W. Greiner, J.Y. Park, W. Scheid, *Nuclear Molecules* (World Scientific, Singapore, 1995).
18. T.M. Shneidman, G.G. Adamian, N.V. Antonenko, S.P. Ivanova, R.V. Jolos, W. Scheid, Phys. Rev. C **65**, 064302 (2002).
19. A. Krasznahorkay *et al.*, Phys. Rev. Lett. **80**, 2073 (1998); P.G. Thirolf, D. Habs, Prog. Part. Phys. **49**, 325 (2002).
20. J.F. Berger, M. Girod, D. Gogny, Nucl. Phys. A **502**, 85c (1989); M.K. Pal, Nucl. Phys. A **556**, 201 (1993); K. Rutz *et al.*, Nucl. Phys. A **590**, 680 (1994); A. Sobiczewski *et al.*, Nucl. Phys. A **473**, 77 (1987); V.V. Pashkevich, Nucl. Phys. A **169**, 275 (1971); P. Möller, S.G. Nilsson, R.K. Sheline, Phys. Lett. B **40**, 329 (1972).
21. V.M. Strutinsky, *Proceedings of the 2nd International Symposium on Physics and Chemistry of Fission* (IAEA, Vienna, 1969) p. 155.
22. W. Lang, H.G. Clerc, H. Wohlfarth, H. Schrader, K.H. Schmidt, Nucl. Phys. A **345**, 34 (1980).
23. C. Schmitt *et al.*, Nucl. Phys. A **430**, 21 (1984).